

pubs.acs.org/NanoLett Letter

Time-resolved ARPES Determination of a Quasi-Particle Band Gap and Hot Electron Dynamics in Monolayer MoS₂

Woojoo Lee, Yi Lin, Li-Syuan Lu, Wei-Chen Chueh, Mengke Liu, Xiaoqin Li, Wen-Hao Chang, Robert A. Kaindl, and Chih-Kang Shih*



Cite This: Nano Lett. 2021, 21, 7363-7370



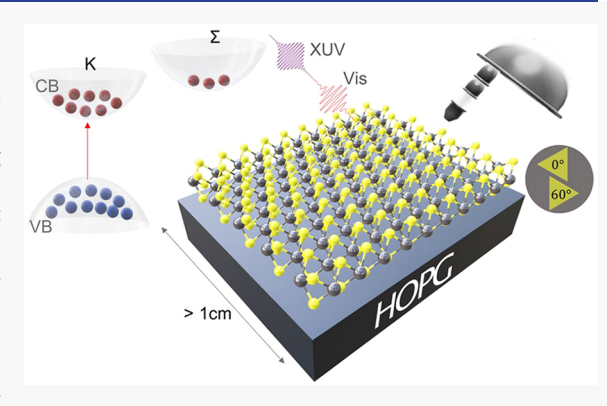
ACCESS

Metrics & More

Article Recommendations

SI Supporting Information

ABSTRACT: The electronic structure and dynamics of 2D transition metal dichalcogenide (TMD) monolayers provide important underpinnings both for understanding the many-body physics of electronic quasi-particles and for applications in advanced optoelectronic devices. However, extensive experimental investigations of semiconducting monolayer TMDs have yielded inconsistent results for a key parameter, the quasi-particle band gap (QBG), even for measurements carried out on the same layer and substrate combination. Here, we employ sensitive time- and angle-resolved photoelectron spectroscopy (trARPES) for a high-quality large-area MoS_2 monolayer to capture its momentum-resolved equilibrium and excited-state electronic structure in the weak-excitation limit. For monolayer MoS_2 on graphite, we obtain QBG values of ≈2.10 eV at 80 K and of ≈2.03 eV at 300 K, results well-corroborated by the scanning tunneling spectroscopy (STS) measurements on the same material.



KEYWORDS: Transition metal dichalcogenide (TMD), MoS_2 , monolayer, XUV-trARPES, electronic structure, exciton

he emergence of monolayer (ML) transition metal dichalcogenides (TMDs) has opened up new frontiers for materials science and novel devices. 1-7 As a consequence of the extreme two-dimensional (2D) geometry, Coulomb or dielectric screening is significantly reduced, which results in remarkably large exciton binding energies as well as important implications for the formation of exotic quantum states. Reduced Coulomb or dielectric screening also impacts the quasi-particle electronic structure, including the quasi-particle band gap (QBG), which is also referred to as the quasi-particle renormalization effect. Accurate knowledge of the quasiparticle electronic structure is critical for designing novel electronic and photonic devices. Moreover, any error incurred in the QBG determination directly translates into an error in the determination of the exciton binding energy, another key parameter in designing photonic systems to realize novel quantum phenomena such as exciton condensates. The quasiparticle renormalization effect, on the one hand, adds to diverse toolsets to tailor electronic structures of TMDs.8 On the other hand, however, it presents challenges to achieving an accurate determination of the QBG of TMDs since the QBG determined on one sample structure cannot be directly translated to another sample structure.

Previous extensive efforts to determine the QBG have not yielded consistent results. For example, in the case of monolayer WS₂ on SiO₂, substantial differences in the QBG

were reported^{21,22} when derived from optical luminescence and absorption spectroscopy. Moreover, in the case of MoS₂ on SiO2, optical studies based on the excitonic Rydberg yielded a smaller QBG than the value acquired from gate-tuned photoluminescence excitation (PLE) spectra. 18 It is unclear whether such a discrepancy reflects the difference in the measurements themselves which incur effects that are not yet accurately accounted for or it is simply due to the sample variability. Regardless, neither techniques probe quasi-particle band structures directly. In principle, scanning tunneling microscopy (STM) can probe the QBG directly. In this case, however, the literature shows a QBG value ranging from 1.9 to 2.4 eV, even for monolayer MoS_2 on graphite (the same sample structure). ^{8,24-30} As analyzed by Zhang et al., ³¹ the tunneling decay constants for different critical points (e.g., Γ vs K) in the TMD monolayer differ significantly, resulting in orders of magnitude difference in the tunneling probability. Thus, a conventional approach may not have enough sensitivity to accurately determine the band edge location.

Received: July 9, 2021 Revised: August 19, 2021 Published: August 23, 2021





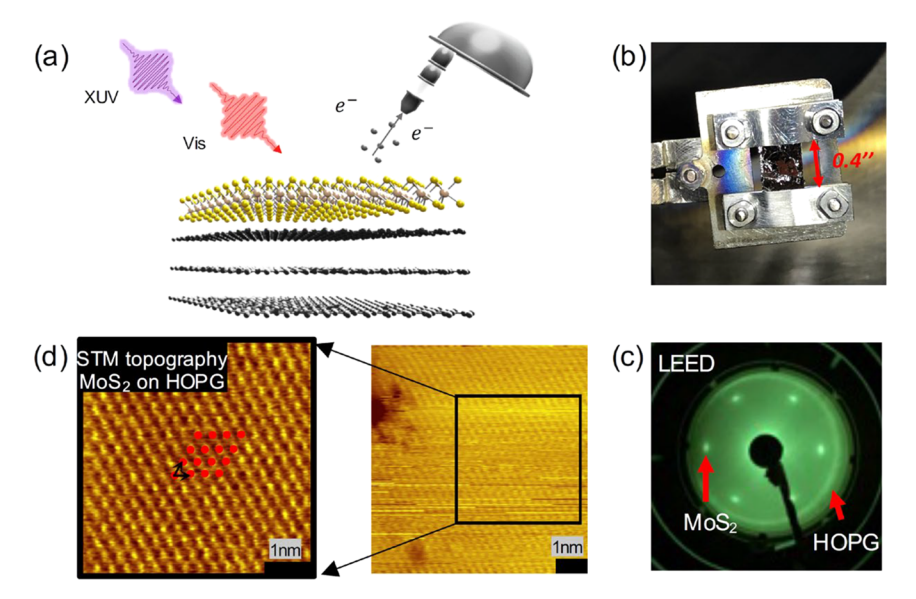


Figure 1. Large-scale oriented MoS_2 monolayers on HOPG and the transient probe scheme. (a) Illustration of the time-resolved ARPES of the photoexcited monolayer's electronic structure. (b) Sample mounted for photoemission with a ≈ 1 cm (0.4 in.) accessible lateral width. (c and d) LEED images (68 eV bias voltage) and STM topography, respectively, of the MoS_2 monolayer, confirming a high surface quality and crystalline orientation.

Although this difficulty can be overcome by employing a sophisticated variable-z tunneling spectroscopic approach, ³¹ it has not been widely adopted. Moreover, it is not a direct k-space measurement, and the band edge location is inferred only indirectly from the behaviors of different thresholds. In this regard, time-resolved angle-resolved photoelectron spectroscopy (trARPES) would be an ideal tool since it can reveal the k-resolved electronic states in both the valence and conduction bands. We emphasize, however, that there are several caveats. In the trARPES measurements of excited states, one needs to disentangle quasi-particle electrons from other forms of many-body states such as excitons. Moreover, one needs to separate the additional renormalization effect due to photoexcited carriers other than the substrate.

To implement the trARPES measurement of quasi-particle band structures for monolayer TMDs, there are several technical challenges. First, to resolve the equilibrium and excited states at the K-valley, extreme-UV (XUV) photons are necessary for photoemission, precluding the use of the more common trARPES approaches using a 6 eV probe. Second, high-quality trARPES requires large-area ML samples that are laterally homogeneous with an atomically clean surface and well-defined in-plane crystallographic orientation. Finally, strong excitation can lead to strong energy renormalization, which would preclude a reliable QBG determination. Due to these challenges, only a few studies of ML-TMDs using XUV trARPES have been reported. 32-37 In the previous investigations, ML-TMD samples were either prepared by physical vapor deposition (PVD) or chemical vapor deposition (CVD) on graphene or metallic substrates, 32-34,37 or as large-area exfoliated MLs derived from single crystals.35,36 While this enabled important insights into electronic dynamics, the sensitivity or resolution has so far been insufficient to enable a precise determination of the QBG. We note that the recent use of micro-trARPES with an ultrahigh repetition rate has achieved successful characterizations of exciton dynamics with a high sensitivity on mechanically exfoliated monolayer WSe₂.³⁸

In this work, by utilizing a wafer-scale MoS_2 monolayer with a well-aligned in-plane orientation along with sensitive XUV-trARPES with high energy and momentum resolution, we resolve the quasi-particle equilibrium and excited electronic structures at different critical points. From such measurements, the QBG in monolayer MoS_2 on graphite is unambiguously determined. Interestingly, the QBG is well corroborated by scanning tunneling spectroscopy (STS) measurements on the same sample structure.

Panels a and b in Figure 1 depict the sample structure and size of the wafer-scale well-aligned monolayer MoS₂ and the transient probe scheme, respectively. We first epitaxially grow a MoS₂ ML on a 2 in. diameter sapphire wafer using CVD. The "substrate guided growth" procedure is then utilized, 39-41 providing significant improvements in terms of reducing the defect density and obtaining monolayers with a well-aligned orientation (cf. Figure S2). HOPG was chosen as a conductive support substrate to prevent the buildup of a surface photovoltage during photoemission 35,38,42 and to eliminate tip-induced band bending during STM measurements. 43-46 After removing the poly(methyl methacrylate) (PMMA) polymer used for the transfer, the sample was further annealed in ultrahigh-vacuum (UHV) to remove the PMMA residue. Additional details of the sample preparation are provided in Supporting Information Figure S3. We note that while largearea TMD MLs with a similar transfer method were previously used in static ARPES, 47-49 orientational variations of the ML flakes in those studies resulted in an admixture of different momentum-space structures that complicated the band structure determination.

As shown in Figure 1c, low-energy electron diffraction (LEED) measurements of our sample reveal a well-defined pattern that confirms the high crystalline quality of the transferred MoS₂ monolayer, corresponding to a high orientational alignment of the domains and their twin pairs. The ring pattern is produced by the HOPG. The LEED pattern remained stable while the electron beam was scanned across the sample, indicating an aligned and clean surface over the

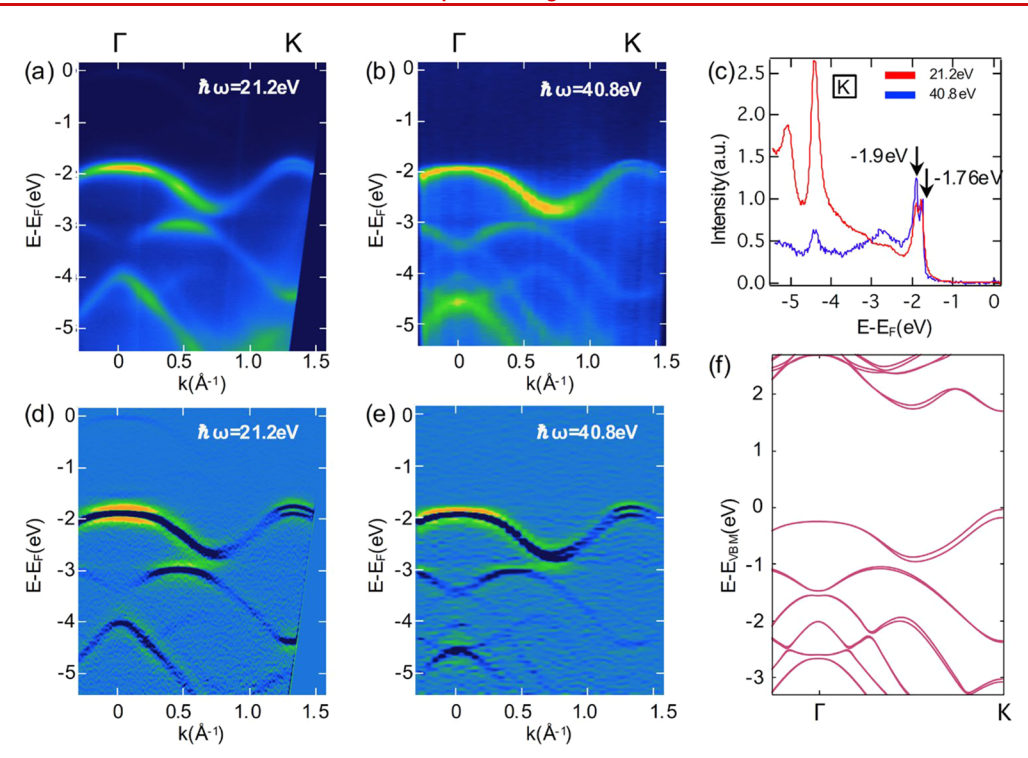


Figure 2. Static ARPES maps of ML MoS₂ on HOPG. Occupied band structure obtained with a He lamp source at (a) 21.2 and (b) 40.8 eV photon energies. (c) EDCs at the K-point integrated over $\pm 0.025 \, \text{Å}^{-1}$ for 21.2 (red) and 40.8 eV (blue) photon energy. The data indicates a spinorbit splitting of 140 \pm 4 meV. (d and e) Second-derivative images corresponding to panels a and b, respectively, for better visualization of the dispersion. (f) Electronic band structure of a free-standing MoS₂ monolayer calculated via DFT using the Quantum ESPRESSO package.

whole sample area. STM images shown in Figure 1d were obtained at 77 K, revealing a lattice constant of 3.17 \pm 0.03 Å that is in agreement with the well-accepted value of 3.16 Å. We note that while the cleaning procedure left minimal traces of residue on the surface, the amounts were too small to impact ARPES, trARPES, and STM/S investigations of the quasiparticle electronic structure. $^{35,36,47-50}$

Panels a and b of Figure 2 show ARPES maps of the momentum-space electronic structure in the valence band, which we probed via static ARPES using a He lamp excitation source with 21.2 and 40.8 eV photon energies, respectively. Corresponding K-point energy distribution curves (EDCs) are indicated in Figure 2c. Each photon energy offers distinct advantages and drawbacks; the 21.2 eV line is brighter but has different sensitivities for dissimilar bands, whereas the 40.8 eV line is about two orders of magnitude weaker yet yields a more uniform photoionization cross-section for all bands. 51 Panels d and e of Figure 2 show the respective second-derivative images for improved contrast. The states near the valence band maximum (VBM) at Γ and K are resolved well, revealing a Kvalley spin-orbit splitting of 140 \pm 4 meV and the Γ valley located ≈130 meV below the VBM. The deeper valence bands were better revealed with the 40.8 eV photons, resulting in a band structure that compares very well with that calculated via density functional theory (DFT). The latter is shown in Figure 2f for a free-standing single-layer MoS2. Importantly, we also find that the atomically clean surface can be recovered through UHV annealing even after exposure to ambient air. This results in consistent ARPES spectra (see Figure S4) and enables straightforward transfer between experimental setups.

We investigated the excited-state electronic structure and dynamics of the MoS₂ monolayers using a high-repetition-rate XUV-trARPES setup, ⁵² which provided direct access to the

electronic bandgap via excitation into otherwise unoccupied levels. In these experiments, the MoS₂ ML was excited above the gap with 2.2 eV pump pulses from a frequency-doubled optical parametric amplifier at a 25 kHz repetition rate with an absorbed fluence of \approx 26 μ J/cm². Subsequently, p-polarized XUV probe pulses at 22.3 eV were used for the photoemission. Figure 3a shows the transient band structure at 300 K measured at a pump–probe delay time of $\Delta t = 0.13$ ps, evidencing the observation of both the valence band and the pump-excited states near the conduction band minimum (CBM).

Figure 3b shows plots of corresponding EDCs around the Kpoint for a later time delay of $\Delta t = 1.27$ ps when the carriers have relaxed toward the CBM for two different sample temperatures of 80 and 300 K. We noted that near $\Delta t = 0$ there is a rapid downshift of the K-point valence band edge by \approx 0.1 eV within about 200 fs (see Figure 4), with the conduction band edge shifting in the same direction. The energies then remain nearly steady on the longer picosecond time scale. Since both valence and conduction band states are concurrently affected, the shifts nearly cancel out, as shown in Figure 4c and d, and the determination of the quasi-particle bandgap is not significantly influenced by this effect. The origin of this downward shift and other many-body effects (including the excitonic effect) in the trARPES process are outside the scope of the current paper and will be presented elsewhere. Here we primarily focus on the determination of the QBG. The valence band spin-orbit splitting of ≈140 meV at the Kpoint is well resolved at 80 K and broadened at 300 K. The CBM energy at the K-point decreases with temperature from 0.25 eV at 80 K to 0.18 eV at 300 K while, within the energy resolution, the K-point VBM remains steady at -1.85 eV. The energy differences between the VBM and the transiently

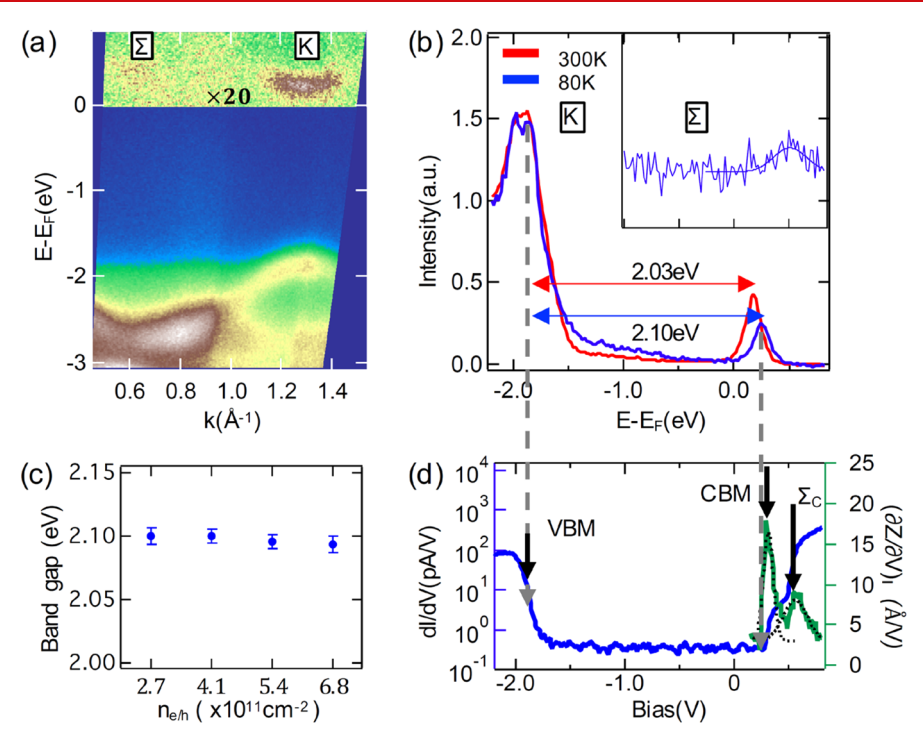


Figure 3. Time-resolved ARPES and scanning tunneling spectroscopy (STS) of monolayer MoS₂ on HOPG. (a) Energy-momentum dispersion along Γ – K of the photoexcited monolayer for a $\Delta t = 0.13$ ps time delay (integrated over ± 0.2 ps) and a 300 K lattice temperature. The sample was excited with 2.2 eV pump pulses and probed via extreme-UV (XUV) pulses around 22.3 eV. The transiently occupied conduction band is clearly visible at the K- and Σ-points. (b) EDCs around the K-point for two sample temperatures and a longer time delay of $\Delta t = 1.27$ ps, integrated over ± 0.5 ps, and $\Delta k = 0.05$ Å⁻¹. A quasi-particle band gap of 2.03 ± 0.02 eV at 300 K was obtained, based on Gaussian fits with the standard deviation, increasing to 2.10 ± 0.02 eV at 80 K. The inset shows the EDC at the Σ-point measured 0.13 ps after excitation with 1.8 eV pump pulses, integrated over ± 0.15 ps, and $\Delta k = 0.25$ Å⁻¹. (c) Pump-power dependence of the K-point quasi-particle band gap at 80 K. (d) STS measured at 77 K representing the differential conductance dI/dV (blue) acquired at a constant height and the $(\partial Z/\partial V)_I$ signal (green) acquired at a constant current in comparison to the valence band maximum (VBM) and the conduction band minimum (CBM) derived from the trARPES measurements; $(\partial Z/\partial V)_I$ is used to distinguish thresholds (in this case Σ-point versus K-point). A detailed description can be found in Figure S6 as well as ref 31.

occupied CBM, indicated also in Figure 3b, thus allow us to directly determine the bandgap. This results in QBG values of 2.10 ± 0.02 eV at an 80 K lattice temperature and 2.03 ± 0.02 eV at 300 K for the MoS₂ monolayer.

Importantly, as shown in Figure 3c, the quasi-particle gap value remains nearly constant as a function of the excitation density. This highlights the negligible influence of pump-induced bandgap renormalization and attests to the validity of our analysis in Figure 4; in the time-delayed spectra, the transient incident pump fluence after $\Delta t = 0$ will increase in $\Delta t = 200$ fs due to the finite pulse width, during which time the trend of the gap size should be equivalent to the one shown in Figure 3c. Unlike the previous study of $MoS_2/graphene$, which exhibited a large bandgap renormalization as a function of the excitation fluence,³³ our measurements were performed at significantly smaller excitation levels. To be specific, in such a small photoexcitation, the dielectric screening effect^{10,11} from the HOPG substrate becomes predominant rather than the screening from photoexcited free carriers.

Despite the distinctive capability of trARPES to verify unoccupied electronic structures directly, it is nontrivial to distinguish the exciton and free carrier states from photoemission signals (especially when energy resolution is limited). The theoretical work of Rustagi and Kemper⁵³ showed that the exciton dispersion obtained from the photoemission has a downward parabolic shape at low temperatures. This suggests that exciton and free carrier states can be distinguished using

the shape of their dispersion. However, concurrently they showed that at high temperatures, thermally excited exciton states with a nonzero center-of-mass can form an upward parabolic dispersion like free carriers so that under limitedenergy resolution a CB photoemission signal can be weighted with a hot exciton signal. In our experimental work, we check the "apparent" effective masses at two different temperatures, 80 and 300 K, and find an effective mass of \sim 0.7 m₀ at 80 K and that of $\sim 1.2 \text{ m}_0$ at 300 K. The value of 0.7 m₀ is consistent with the electron effective mass derived from the measurement of the temperature dependence of Shubnikov-de Haas (SdH) oscillations as a function of the magnetic field.⁵⁴ This confirms that the observed dispersion at 80 K corresponds to that of the free electrons, with minimal contributions from hot excitons carrying nonzero center-of-mass (COM) momentum. On the other hand, at 300 K a larger "apparent" effective mass suggests a mixture of free electrons and hot excitons (hot excitons would have an apparent effective mass of $m^* = m_e + m_h = 1.4$ m_0). See Supporting Information Figure S5 for more details. This might be due to the fact that "hot excitons" decay slower at 300 K than that at 80 K. Nevertheless, as we discussed in Supporting Information Figure S6, at the above-gap excitation (2.2 eV), the zero-COM momentum exciton population is always much smaller than the free carrier contribution. Thus, the determination of the CBM position is not significantly affected by the presence of the hot exciton. Since the scope of this paper is on the accurate determination of the quasi-particle

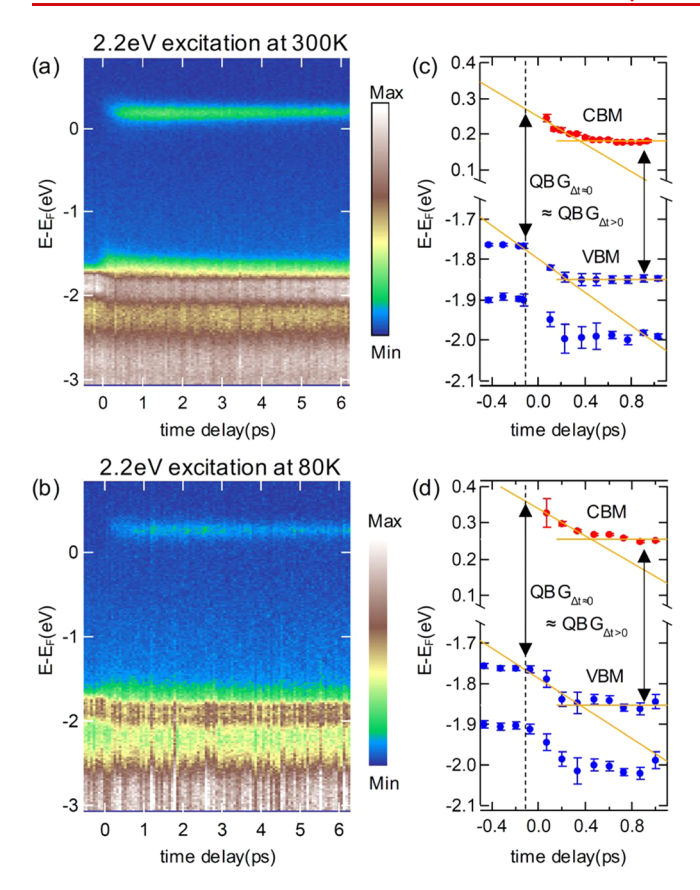


Figure 4. (a and b) Time-dependent VB downward shift at the K-point at 300 and 80 K, respectively, as seen in trARPES maps of the energy-dependent photoelectron intensity versus the pump-probe time delay. The downward VB shift on the order of 0.1 ± 0.02 eV occurs near time zero (near -2 eV). (c and d) Extracted peak position at the K-point conduction (red) and valence (blue) bands near time zero at 300 and 80 K respectively. The size of the CB shift was obtained by extrapolating (orange solid lines) the peaks near time zero. From the extrapolation, the QBG at 300 K was obtained as 2.04 \pm 0.07 eV and that at 80 K QBG was obtained as 2.12 \pm 0.03 eV, which is consistent with the QBG in the main text within the error bar. Also, the invariant QBG value when the pump power in Figure 3c was varied supports that the QBG change is negligible in the lower fluence regime (corresponding to times near time zero).

band structure, a more in-depth discussion of excitonic effects as well as other forms of many-body effects will be presented elsewhere.

We now compare the MoS₂ monolayer electronic structure derived from trARPES at 80 K with that determined from STS measurements acquired at 77 K. As shown in Figure 3d, in the STS measurements the VBM occurs at -1.84 eV and the CBM occurs at 0.31 eV. This results in an STS-derived bandgap of 2.15 ± 0.06 eV, which is in excellent agreement with the value determined from trARPES. These mutually consistent results also provide a resolution to the controversies regarding the QBG initiated by different STM studies.^{8,24-31,43} In addition, the STS measurements further identify a second threshold located at 0.2 ± 0.05 eV above the CBM. The two thresholds can be more clearly identified in the $(\partial Z/\partial V)_I$ spectrum (shown as green curve), which is acquired by keeping the current constant and sweeping the bias while observing the change in the tip-to-sample separation. As discussed previously in ref 31 (also briefly summarized in Supporting Information Figure S7), the sharp peaks in the $(\partial Z/\partial V)_I$ spectrum are

associated with the thresholds originating from different valleys in the BZ (albeit not a direct k-resolved method). The lower threshold is simply the CBM at the K-point, while the second threshold above it is assigned as $\Sigma_{\rm c}$ (often referred to as Q_c). In turn, the trARPES signals in the inset of Figure 3b also reveal the Σ state at 0.55 \pm 0.03 eV, although the count rate and thus the transient quasi-particle occupation is much lower than those at the K-point.

Finally, we discuss the excited-state dynamics. Figure 5a shows the transient ARPES signals at 80 K around the K-point

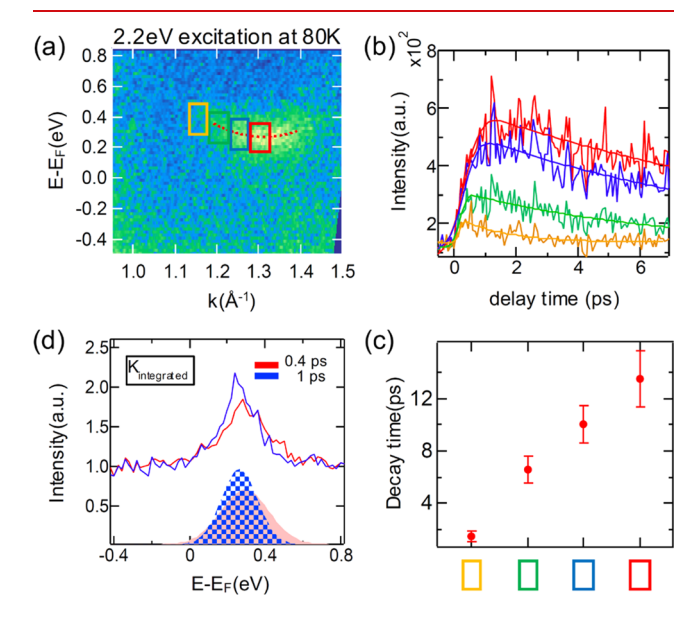


Figure 5. Intravalley dynamics around K-point. (a) Parabolic shape of the E-k dispersion at the K-point conduction band observed with trARPES. (b) Photoelectron intensity versus time delay spectra for different points along the the parabolic shape dispersion per the colored box areas of panel a. (c) Decay time of the states in the colored boxes. (d) Momentum-integrated EDC around K. The area of the curve, which represents the photoexcited electrons in the K-valley conduction band, changes less than $\sim 3\%$ during the initial relaxation.

for a representative time delay of $\Delta t = 0.4$ ps, clearly evidencing an upward parabolic dispersion corresponding to the conduction band minimum. To understand the early dynamics, we plot the time-dependent photoemission signals from four different momentum regions near the K-point and its decay time in panels b and c of Figure 5. Carriers at high energies (yellow box) exhibit dynamics that peak at an early time delay of ≈ 0.3 ps, with a subsequent rapid decay on a ≈ 1.5 ps time scale. Approaching the K-point minimum, the dynamics systematically peak at later times and then decay with longer time constants (green and blue box). Finally, at the K-point CBM the dynamics exhibit a peak density around ≈ 1.2 ps, followed by a decay with a ≈ 13 ps time constant. This trend indicates the successive electron scattering from higher to lower energies, which is consistent with a hot electron decay down to the local minimum in momentum space.⁵⁵

Figure 5d shows two K-valley-integrated EDC spectra acquired at $\Delta t = 0.4$ and 1.0 ps, respectively. The areas below each spectral peak are identical within 3%, indicating that nearly all the hot electrons in the K-valley are cooled to the CBM and additional contributions from intervalley-scattered Σ -valley ($\Sigma_{\rm c}$) electrons are minor. We notice that the strength of the $\Sigma_{\rm c}$ occupation will vary with the

experimental conditions.³⁸ For the transient photoelectron signal at Σ_c that reveals efficient ultrafast intervalley scattering near time zero with a fast decay of ~500 fs, ^{56,57} see Supporting Information Figure S8.

In conclusion, the successful fabrication of large-scale monolayer MoS2 on HOPG was combined with static and time-resolved surface probes to investigate its equilibrium and excited-state electronic structure. Equilibrium measurements evidence a uniform in-plane orientation and an atomically clean surface across the sample, with a band structure consistent with DFT calculations. Sensitive time-resolved XUV ARPES provided concurrent access to the valence band and transiently excited conduction band states, yielding a direct measure of the quasi-particle bandgap in ML MoS₂. We found the resulting value to be in remarkable agreement with the electronic bandgap determined from STS measurements on the same sample structure. Furthermore, XUV-trARPES reveals ultrafast intra- and intervalley dynamics and a parabolic conduction band minimum around the K-point with the excitonic influence. Future experiments utilizing the combination of wafer-scale TMDs and sensitive trARPES can fully access their complex electron dynamics in time, energy, and momentum to guide the search for the new valley and exciton physics and devices based on TMD monolayers and heterostructures.

ASSOCIATED CONTENT

Supporting Information

The Supporting Information is available free of charge at https://pubs.acs.org/doi/10.1021/acs.nanolett.1c02674.

Regular and time-resolved ARPES experimental methods, computational methods, a large discrepancy of the bandgap size in STM studies, optical characterization of ML-MoS₂, wet-transfer procedure, ML-MoS₂ air stability, effective masses measured at the K-point, bandgap determination in the trARPES measurements, $(\partial Z/\partial V)_I$ technique for critical points identification, and transient photoelectron intensity (exciton and free carrier mixture) (PDF)

AUTHOR INFORMATION

Corresponding Author

Chih-Kang Shih — Department of Physics, The University of Texas at Austin, Austin, Texas 78712, United States; oorcid.org/0000-0003-2734-7023; Email: shih@physics.utexas.edu

Authors

Woojoo Lee – Department of Physics, The University of Texas at Austin, Austin, Texas 78712, United States

Yi Lin – Materials Sciences Division, Lawrence Berkeley National Laboratory, Berkeley, California 94720, United States

Li-Syuan Lu – Department of Electrophysics, National Chiao Tung University, Hsinchu 30010, Taiwan

Wei-Chen Chueh – Department of Electrophysics, National Chiao Tung University, Hsinchu 30010, Taiwan

Mengke Liu – Department of Physics, The University of Texas at Austin, Austin, Texas 78712, United States

Xiaoqin Li — Department of Physics, The University of Texas at Austin, Austin, Texas 78712, United States

Wen-Hao Chang — Department of Electrophysics, National Chiao Tung University, Hsinchu 30010, Taiwan; Center for Emergent Functional Matter Science (CEFMS), National Chiao Tung University, Hsinchu 30010, Taiwan; orcid.org/0000-0003-4880-6006

Robert A. Kaindl — Materials Sciences Division, Lawrence Berkeley National Laboratory, Berkeley, California 94720, United States; Department of Physics and CXFEL Laboratory, Arizona State University, Tempe, Arizona 85287, United States

Complete contact information is available at: https://pubs.acs.org/10.1021/acs.nanolett.1c02674

Notes

The authors declare no competing financial interest.

ACKNOWLEDGMENTS

This research was primarily supported by the National Science Foundation through the Center for Dynamics and Control of Materials via an NSF MRSEC under cooperative agreement no. DMR-1720595 and the facility supported by MRSEC. C.K.S. also acknowledges NSF-DMR 1808751, the Welch Foundation F-1672, and the US Airforce FA2386-18-1-4097. X.L. acknowledges the Welch Foundation F-1662. Work at Lawrence Berkeley National Laboratory by Y.L. and R.A.K. including trARPES was supported by the U.S. Department of Energy (DOE), Office of Science, Office of Basic Energy Sciences, Materials Sciences and Engineering Division under contract no. DE-AC02-05-CH11231 (Ultrafast Materials Science Program No. KC2203). L.W.-H.C. acknowledges support from the Ministry of Science and Technology of Taiwan (MOST-107-2112-M-009-024-MY3 and MOST-108-2119-M-009-011-MY3) and the Center for Emergent Functional Matter Science (CEFMS) of NCTU supported by the Ministry of Education of Taiwan.

REFERENCES

- (1) Wang, Q. H.; Kalantar-Zadeh, K.; Kis, A.; Coleman, J. N.; Strano, M. S. Electronics and optoelectronics of two-dimensional transition metal dichalcogenides. *Nat. Nanotechnol.* **2012**, *7*, 699.
- (2) Butler, S. Z.; Hollen, S. M.; Cao, L.; Cui, Y.; Gupta, J. A.; Gutiérrez, H. R.; Heinz, T. F.; Hong, S. S.; Huang, J.; Ismach, A. F.; Johnston-Halperin, E.; Kuno, M.; Plashnitsa, V. V.; Robinson, R. D.; Ruoff, R. S.; Salahuddin, S.; Shan, J.; Shi, L.; Spencer, M. G.; Terrones, M.; Windl, W.; Goldberger, J. E. Progress, Challenges, and Opportunities in Two-Dimensional Materials Beyond Graphene. *ACS Nano* 2013, 7, 2898.
- (3) Geim, A. K.; Grigorieva, I. V. Van der Waals heterostructures. *Nature* **2013**, 499, 419.
- (4) Xia, F.; Wang, H.; Xiao, D.; Dubey, M.; Ramasubramaniam, A. Two-dimensional material nanophotonics. *Nat. Photonics* **2014**, *8*, 899.
- (5) Mak, K. F.; Shan, J. Photonics and optoelectronics of 2D semiconductor transition metal dichalcogenides. *Nat. Photonics* **2016**, 10, 216
- (6) Novoselov, K. S.; Mishchenko, A.; Carvalho, A.; Neto, A. H. C. 2D materials and van der Waals heterostructures. *Science* **2016**, 353, aac9439.
- (7) Rivera, P.; Yu, H.; Seyler, K. L.; Wilson, N. P.; Yao, W.; Xu, X. Interlayer valley excitons in heterobilayers of transition metal dichalcogenides. *Nat. Nanotechnol.* **2018**, *13*, 1004.
- (8) Shi, J.; Liu, M.; Wen, J.; Ren, X.; Zhou, X.; Ji, Q.; Ma, D.; Zhang, Y.; Jin, C.; Chen, H.; Deng, S.; Xu, N.; Liu, Z.; Zhang, Y. All Chemical Vapor Deposition Synthesis and Intrinsic Bandgap Observation of MoS₂/Graphene Heterostructures. *Adv. Mater.* **2015**, *27*, 7086.

- (9) Zhang, Q.; Chen, Y.; Zhang, C.; Pan, C.-R.; Chou, M.-Y.; Zeng, C.; Shih, C.-K. Bandgap renormalization and work function tuning in MoSe₂/hBN/Ru(0001) heterostructures. *Nat. Commun.* **2016**, *7*, 13843.
- (10) Raja, A.; Chaves, A.; Yu, J.; Arefe, G.; Hill, H. M.; Rigosi, A. F.; Berkelbach, T. C.; Nagler, P.; Schüller, C.; Korn, T.; Nuckolls, C.; Hone, J.; Brus, L. E.; Heinz, T. F.; Reichman, D. R.; Chernikov, A. Coulomb engineering of the bandgap and excitons in two-dimensional materials. *Nat. Commun.* **2017**, *8*, 15251.
- (11) Hsu, W.-T.; Quan, J.; Wang, C.-Y.; Lu, L.-S.; Campbell, M.; Chang, W.-H.; Li, L.-J.; Li, X.; Shih, C.-K. Dielectric impact on exciton binding energy and quasiparticle bandgap in monolayer WS₂ and WSe₂. 2D Mater. **2019**, *6*, 025028.
- (12) Steinhoff, A.; Rösner, M.; Jahnke, F.; Wehling, T. O.; Gies, C. Influence of Excited Carriers on the Optical and Electronic Properties of MoS₂. *Nano Lett.* **2014**, *14*, 3743.
- (13) Chernikov, A.; van der Zande, A. M.; Hill, H. M.; Rigosi, A. F.; Velauthapillai, A.; Hone, J.; Heinz, T. F. Electrical Tuning of Exciton Binding Energies in Monolayer WS₂. *Phys. Rev. Lett.* **2015**, *115*, 126802.
- (14) Chernikov, A.; Ruppert, C.; Hill, H. M.; Rigosi, A. F.; Heinz, T. F. Population inversion and giant bandgap renormalization in atomically thin WS₂ layers. *Nat. Photonics* **2015**, *9*, 466.
- (15) Liang, Y.; Yang, L. Carrier Plasmon Induced Nonlinear Band Gap Renormalization in Two-Dimensional Semiconductors. *Phys. Rev. Lett.* **2015**, *114*, 063001.
- (16) Pogna, E. A. A.; Marsili, M.; De Fazio, D.; Dal Conte, S.; Manzoni, C.; Sangalli, D.; Yoon, D.; Lombardo, A.; Ferrari, A. C.; Marini, A.; Cerullo, G.; Prezzi, D. Photo-Induced Bandgap Renormalization Governs the Ultrafast Response of Single-Layer MoS₂. ACS Nano 2016, 10, 1182.
- (17) Liu, B.; Zhao, W.; Ding, Z.; Verzhbitskiy, I.; Li, L.; Lu, J.; Chen, J.; Eda, G.; Loh, K. P. Engineering Bandgaps of Monolayer MoS₂ and WS₂ on Fluoropolymer Substrates by Electrostatically Tuned Many-Body Effects. *Adv. Mater.* **2016**, *28*, 6457.
- (18) Yao, K.; Yan, A.; Kahn, S.; Suslu, A.; Liang, Y.; Barnard, E. S.; Tongay, S.; Zettl, A.; Borys, N. J.; Schuck, P. J. Optically Discriminating Carrier-Induced Quasiparticle Band Gap and Exciton Energy Renormalization in Monolayer MoS₂. *Phys. Rev. Lett.* **2017**, *119*, 087401.
- (19) Cunningham, P. D.; Hanbicki, A. T.; McCreary, K. M.; Jonker, B. T. Photoinduced Bandgap Renormalization and Exciton Binding Energy Reduction in WS₂. ACS Nano **2017**, 11, 12601.
- (20) Katoch, J.; Ulstrup, S.; Koch, R. J.; Moser, S.; McCreary, K. M.; Singh, S.; Xu, J.; Jonker, B. T.; Kawakami, R. K.; Bostwick, A.; Rotenberg, E.; Jozwiak, C. Giant spin-splitting and gap renormalization driven by trions in single-layer WS₂ /h-BN heterostructures. *Nat. Phys.* **2018**, *14*, 355.
- (21) Ye, Z.; Cao, T.; O'Brien, K.; Zhu, H.; Yin, X.; Wang, Y.; Louie, S. G.; Zhang, X. Probing excitonic dark states in single-layer tungsten disulphide. *Nature* **2014**, *513*, 214.
- (22) Chernikov, A.; Berkelbach, T. C.; Hill, H. M.; Rigosi, A.; Li, Y.; Aslan, O. B.; Reichman, D. R.; Hybertsen, M. S.; Heinz, T. F. Exciton Binding Energy and Nonhydrogenic Rydberg Series in Monolayer WS₂. Phys. Rev. Lett. **2014**, 113, 076802.
- (23) Hill, H. M.; Rigosi, A. F.; Roquelet, C.; Chernikov, A.; Berkelbach, T. C.; Reichman, D. R.; Hybertsen, M. S.; Brus, L. E.; Heinz, T. F. Observation of Excitonic Rydberg States in Monolayer MoS₂ and WS₂ by Photoluminescence Excitation Spectroscopy. *Nano Lett.* **2015**, *15*, 2992.
- (24) Trainer, D. J.; Putilov, A. V.; Di Giorgio, C.; Saari, T.; Wang, B.; Wolak, M.; Chandrasena, R. U.; Lane, C.; Chang, T.-R.; Jeng, H.-T.; Lin, H.; Kronast, F.; Gray, A. X.; Xi, X.; Nieminen, J.; Bansil, A.; Iavarone, M. Inter-Layer Coupling Induced Valence Band Edge Shift in Mono- to Few-Layer MoS₂. Sci. Rep. **2017**, *7*, 40559.
- (25) Zhang, C.; Johnson, A.; Hsu, C.-L.; Li, L.-J.; Shih, C.-K. Direct Imaging of Band Profile in Single Layer MoS₂ on Graphite: Quasiparticle Energy Gap, Metallic Edge States, and Edge Band Bending. *Nano Lett.* **2014**, *14*, 2443.

- (26) Huang, Y. L.; Chen, Y.; Zhang, W.; Quek, S. Y.; Chen, C.-H.; Li, L.-J.; Hsu, W.-T.; Chang, W.-H.; Zheng, Y. J.; Chen, W.; Wee, A. T. S. Bandgap tunability at single-layer molybdenum disulphide grain boundaries. *Nat. Commun.* **2015**, *6*, 6298.
- (27) Koós, A. A.; Vancsó, P.; Magda, G. Z.; Osváth, Z.; Kertész, K.; Dobrik, G.; Hwang, C.; Tapasztó, L.; Biró, L. P. STM study of the MoS₂ flakes grown on graphite: A model system for atomically clean 2D heterostructure interfaces. *Carbon* **2016**, *105*, 408.
- (28) Liu, X.; Balla, I.; Bergeron, H.; Campbell, G. P.; Bedzyk, M. J.; Hersam, M. C. Rotationally Commensurate Growth of MoS_2 on Epitaxial Graphene. *ACS Nano* **2016**, *10*, 1067.
- (29) Lu, C.-I.; Butler, C. J.; Huang, J.-K.; Hsing, C.-R.; Yang, H.-H.; Chu, Y.-H.; Luo, C.-H.; Sun, Y.-C.; Hsu, S.-H.; Yang, K.-H. O.; Wei, C.-M.; Li, L.-J.; Lin, M.-T. Graphite edge controlled registration of monolayer MoS₂ crystal orientation. *Appl. Phys. Lett.* **2015**, *106*, 181904.
- (30) Ko, W.; Hus, S. M.; Li, X.; Berlijn, T.; Nguyen, G. D.; Xiao, K.; Li, A.-P. Tip-induced local strain on MoS₂/graphite detected by inelastic electron tunneling spectroscopy. *Phys. Rev. B: Condens. Matter Mater. Phys.* **2018**, 97, 125401.
- (31) Zhang, C.; Chen, Y.; Johnson, A.; Li, M.-Y.; Li, L.-J.; Mende, P. C.; Feenstra, R. M.; Shih, C.-K. Probing Critical Point Energies of Transition Metal Dichalcogenides: Surprising Indirect Gap of Single Layer WSe₂. *Nano Lett.* **2015**, *15*, 6494.
- (32) Grubišić Čabo, A.; Miwa, J. A.; Grønborg, S. S.; Riley, J. M.; Johannsen, J. C.; Cacho, C.; Alexander, O.; Chapman, R. T.; Springate, E.; Grioni, M.; Lauritsen, J. V.; King, P. D. C.; Hofmann, P.; Ulstrup, S. Observation of Ultrafast Free Carrier Dynamics in Single Layer MoS₂, Nano Lett. **2015**, 15, 5883.
- (33) Ustrup, S.; Čabo, A. G.; Miwa, J. A.; Riley, J. M.; Grønborg, S. S.; Johannsen, J. C.; Cacho, C.; Alexander, O.; Chapman, R. T.; Springate, E.; Bianchi, M.; Dendzik, M.; Lauritsen, J. V.; King, P. D. C.; Hofmann, P. Ultrafast Band Structure Control of a Two-Dimensional Heterostructure. ACS Nano 2016, 10, 6315.
- (34) Ulstrup, S.; Čabo, A. G.; Biswas, D.; Riley, J. M.; Dendzik, M.; Sanders, C. E.; Bianchi, M.; Cacho, C.; Matselyukh, D.; Chapman, R. T.; Springate, E.; King, P. D. C.; Miwa, J. A.; Hofmann, P. Spin and valley control of free carriers in single-layer WS₂. *Phys. Rev. B: Condens. Matter Mater. Phys.* **2017**, *95*, 041405.
- (35) Liu, F.; Ziffer, M. E.; Hansen, K. R.; Wang, J.; Zhu, X. Direct Determination of Band-Gap Renormalization in the Photoexcited Monolayer MoS₂. *Phys. Rev. Lett.* **2019**, *122*, 246803.
- (36) Liu, F.; Li, Q.; Zhu, X.-Y. Direct determination of momentum-resolved electron transfer in the photoexcited van der Waals heterobilayer WS₂/MoS₂. *Phys. Rev. B: Condens. Matter Mater. Phys.* **2020**, *101*, 201405.
- (37) Aeschlimann, S.; Rossi, A.; Chávez-Cervantes, M.; Krause, R.; Arnoldi, B.; Stadtmüller, B.; Aeschlimann, M.; Forti, S.; Fabbri, F.; Coletti, C.; Gierz, I. Direct evidence for efficient ultrafast charge separation in epitaxial WS₂/graphene heterostructures. *Science Advances* **2020**, *6*, No. eaay0761.
- (38) Madéo, J.; Man, M. K. L.; Sahoo, C.; Campbell, M.; Pareek, V.; Wong, E. L.; Al-Mahboob, A.; Chan, N. S.; Karmakar, A.; Mariserla, B. M. K.; Li, X.; Heinz, T. F.; Cao, T.; Dani, K. M. Directly visualizing the momentum-forbidden dark excitons and their dynamics in atomically thin semiconductors. *Science* **2020**, *370*, 1199.
- (39) Aljarb, A.; Cao, Z.; Tang, H.-L.; Huang, J.-K.; Li, M.; Hu, W.; Cavallo, L.; Li, L.-J. Substrate Lattice-Guided Seed Formation Controls the Orientation of 2D Transition-Metal Dichalcogenides. *ACS Nano* **2017**, *11*, 9215.
- (40) Hsu, W.-F.; Lu, L.-S.; Kuo, P.-C.; Chen, J.-H.; Chueh, W.-C.; Yeh, H.; Kao, H.-L.; Chen, J.-S.; Chang, W.-H. Monolayer MoS2 Enabled Single-Crystalline Growth of AlN on Si(100) Using Low-Temperature Helicon Sputtering. ACS Appl. Nano Mater. 2019, 2, 1964.
- (41) Yu, H.; Liao, M.; Zhao, W.; Liu, G.; Zhou, X. J.; Wei, Z.; Xu, X.; Liu, K.; Hu, Z.; Deng, K.; Zhou, S.; Shi, J.-A.; Gu, L.; Shen, C.; Zhang, T.; Du, L.; Xie, L.; Zhu, J.; Chen, W.; Yang, R.; Shi, D.; Zhang,

- G. Wafer-Scale Growth and Transfer of Highly-Oriented Monolayer MoS₂ Continuous Films. ACS Nano 2017, 11, 12001.
- (42) Yang, S.-L.; Sobota, J. A.; Kirchmann, P. S.; Shen, Z.-X. Electron propagation from a photo-excited surface: implications for time-resolved photoemission. *Appl. Phys. A: Mater. Sci. Process.* **2014**, *116*, 85.
- (43) Ugeda, M. M.; Bradley, A. J.; Shi, S.-F.; da Jornada, F. H.; Zhang, Y.; Qiu, D. Y.; Ruan, W.; Mo, S.-K.; Hussain, Z.; Shen, Z.-X.; Wang, F.; Louie, S. G.; Crommie, M. F. Giant bandgap renormalization and excitonic effects in a monolayer transition metal dichalcogenide semiconductor. *Nat. Mater.* **2014**, *13*, 1091.
- (44) Feenstra, R. M.; Stroscio, J. A. Tunneling spectroscopy of the GaAs(110) surface. J. Vac. Sci. Technol., B: Microelectron. Process. Phenom. 1987, 5, 923.
- (45) Feenstra, R. M.; Dong, Y.; Semtsiv, M. P.; Masselink, W. T. Influence of tip-induced band bending on tunnelling spectra of semiconductor surfaces. *Nanotechnology* **2007**, *18*, 044015.
- (46) Zhou, X.; Kang, K.; Xie, S.; Dadgar, A.; Monahan, N. R.; Zhu, X.-Y.; Park, J.; Pasupathy, A. N. Atomic-Scale Spectroscopy of Gated Monolayer MoS₂. *Nano Lett.* **2016**, *16*, 3148.
- (47) Lim, Y.-F.; Priyadarshi, K.; Bussolotti, F.; Gogoi, P. K.; Cui, X.; Yang, M.; Pan, J.; Tong, S. W.; Wang, S.; Pennycook, S. J.; Goh, K. E. J.; Wee, A. T. S.; Wong, S. L.; Chi, D. Modification of Vapor Phase Concentrations in MoS_2 Growth Using a NiO Foam Barrier. *ACS Nano* **2018**, *12*, 1339.
- (48) Henck, H.; Ben Aziza, Z.; Pierucci, D.; Laourine, F.; Reale, F.; Palczynski, P.; Chaste, J.; Silly, M. G.; Bertran, F.; Le Fèvre, P.; Lhuillier, E.; Wakamura, T.; Mattevi, C.; Rault, J. E.; Calandra, M.; Ouerghi, A. Electronic band structure of Two-Dimensional WS₂/Graphene van der Waals Heterostructures. *Phys. Rev. B: Condens. Matter Mater. Phys.* **2018**, *97*, 155421.
- (49) Bussolotti, F.; Kawai, H.; Wong, S. L.; Goh, K. E. J. Protected hole valley states in single-layer MoS₂. *Phys. Rev. B: Condens. Matter Mater. Phys.* **2019**, 99, 045134.
- (50) Liu, F.; Wu, W.; Bai, Y.; Chae, S. H.; Li, Q.; Wang, J.; Hone, J.; Zhu, X.-Y. Disassembling 2D van der Waals crystals into macroscopic monolayers and reassembling into artificial lattices. *Science* **2020**, *367*, 903
- (51) Damascelli, A.; Hussain, Z.; Shen, Z.-X. Angle-resolved photoemission studies of the cuprate superconductors. *Rev. Mod. Phys.* **2003**, 75, 473.
- (52) Buss, J. H.; Wang, H.; Xu, Y.; Maklar, J.; Joucken, F.; Zeng, L.; Stoll, S.; Jozwiak, C.; Pepper, J.; Chuang, Y.-D.; Denlinger, J. D.; Hussain, Z.; Lanzara, A.; Kaindl, R. A. A setup for extreme-ultraviolet ultrafast angle-resolved photoelectron spectroscopy at 50-kHz repetition rate. *Rev. Sci. Instrum.* **2019**, *90*, 023105.
- (53) Rustagi, A.; Kemper, A. F. Photoemission signature of excitons. *Phys. Rev. B: Condens. Matter Mater. Phys.* **2018**, *97*, 235310.
- (54) Pisoni, R.; Kormányos, A.; Brooks, M.; Lei, Z.; Back, P.; Eich, M.; Overweg, H.; Lee, Y.; Rickhaus, P.; Watanabe, K.; Taniguchi, T.; Imamoglu, A.; Burkard, G.; Ihn, T.; Ensslin, K. Interactions and Magnetotransport through Spin-Valley Coupled Landau Levels in Monolayer MoS₂. *Phys. Rev. Lett.* **2018**, *121*, 247701.
- (55) Schmuttenmaer, C. A.; Aeschlimann, M.; Elsayed-Ali, H. E.; Miller, R. J. D.; Mantell, D. A.; Cao, J.; Gao, Y. Time-resolved two-photon photoemission from Cu(100): Energy dependence of electron relaxation. *Phys. Rev. B: Condens. Matter Mater. Phys.* **1994**, *50*, 8957.
- (56) Nie, Z.; Long, R.; Sun, L.; Huang, C.-C.; Zhang, J.; Xiong, Q.; Hewak, D. W.; Shen, Z.; Prezhdo, O. V.; Loh, Z.-H. Ultrafast Carrier Thermalization and Cooling Dynamics in Few-Layer MoS₂. ACS Nano 2014, 8, 10931.
- (57) Hein, P.; Stange, A.; Hanff, K.; Yang, L. X.; Rohde, G.; Rossnagel, K.; Bauer, M. Momentum-resolved hot electron dynamics at the 2H MoS₂ surface. *Phys. Rev. B: Condens. Matter Mater. Phys.* **2016**, 94, 205406.